




## Long-term stable compressive elastocaloric cooling system with latent heat transfer

Nora Bachmann <sup>1,2✉</sup>, Andreas Fitger<sup>1</sup>, Lena Maria Maier <sup>1,3</sup>, Andreas Mahlke<sup>1</sup>, Olaf Schäfer-Welsen<sup>1</sup>, Thomas Koch<sup>2</sup> & Kilian Bartholomé <sup>1✉</sup>

Elastocaloric cooling systems can evolve into an environmentally friendly alternative to compressor-based cooling systems. One of the main factors preventing its application is a poor long-term stability of the elastocaloric material. This especially applies to systems that work with tensile loads and which benefit from the large surface area for heat transfer. Exerting compressive instead of tensile loads on the material increases long-term stability—though at the expense of cooling power density. Here, we present a heat transfer concept for elastocaloric systems where heat is transferred by evaporation and condensation of a fluid. Enhanced heat transfer rates allow us to choose the sample geometry more freely and thereby realize a compression-based system showing unprecedented long-term stability of  $10^7$  cycles and cooling power density of  $6270 \text{ W kg}^{-1}$ .

<sup>1</sup>Fraunhofer Institute for Physical Measurement Techniques IPM, Thermal Energy Converters, Freiburg, Germany. <sup>2</sup>Karlsruhe Institute of Technology (KIT), Institute of Internal Combustion Engines IFKM, Karlsruhe, Germany. <sup>3</sup>University of Freiburg, Department of Microsystems Engineering IMTEK, Freiburg, Germany. ✉email: [nora.bachmann@ipm.fraunhofer.de](mailto:nora.bachmann@ipm.fraunhofer.de); [kilian.bartholome@ipm.fraunhofer.de](mailto:kilian.bartholome@ipm.fraunhofer.de)

Refrigeration technology is increasingly used worldwide, resulting in continuous growth of energy consumption<sup>1</sup>. The demand for refrigeration is largely covered by compressor-based systems. These systems work with refrigerants that are often harmful, flammable or restricted due to their greenhouse impact<sup>2</sup>. Meeting the growing demand for cooling technology and at the same time complying with the climate targets set by the Paris Agreement is becoming more and more of a challenge<sup>3</sup>.

Caloric cooling systems, based on the elasto-, magneto-, electro- or barocaloric effect<sup>4</sup>, could be a solution: Caloric cooling systems are potentially more efficient than compressor-based systems<sup>5</sup> and operate without harmful refrigerants. Elastocaloric cooling system (ECS) use elastocaloric materials (ECM) such as nickel-titanium alloys<sup>4</sup>. These alloys are commercially available since they are widely used as shape memory alloys for example in actuators or medical implants. In ECMs, the material's microstructure changes from the austenitic to martensitic phase when exposed to a load, resulting in a reversible temperature change of the material. This "elastocaloric effect" can be induced by tensile and compressive loads<sup>6</sup> as well as by bending and torsion<sup>7</sup>. In ECMs, the mechanical stress induces a reversible, exothermic process that increases the material temperature and allows heat to be released into the environment. When removing the load, the reverse process occurs<sup>4</sup>: The material cools down, heat can be absorbed. By cyclic repetition of this reversible process, thermal energy can be transferred from a cold to a hot reservoir. The heat flow is proportional to the amount of ECM and the load frequency applied to the ECM.

For application in a commercial product, the ECM has to endure the reversible phase transformation process up to billions of times without failing<sup>8,9</sup>. Long-term stability is discussed as a major challenge for ECS<sup>9–13</sup>.

In order to realize an ECM-based cooling system or heat pump, a unidirectional heat flow from heat source to heat sink has to be established. This heat flow is usually implemented by heat conduction between solids, which alternately contact the heat source and the heat sink<sup>14–17</sup>, or by convection with a fluid like air or water being actively pumped alongside the ECM<sup>18–22</sup>. In their ECS, Tušek et al.<sup>21</sup> apply a tensile load on the material and pump water through stacked ECM plates to the heat source and sink. Engelbrecht et al.<sup>20</sup> measured a temperature span of 19.9 K in a further development of this ECS. However, the material failed after 5,500 cycles. The largest temperature span of 28.3 K was recently measured by Snodgrass and Erickson<sup>18</sup> in a three stage setup using liquid water for convective heat transfer. In this ECS, material failure occurred after 300 cycles. In the first published compression-based ECS by Qian et al.<sup>23,24</sup>, water is pumped through tubes made of ECM. Here, a maximum temperature span of 4.7 K and a cooling power of 65 W, corresponding to a specific cooling power of 500–600 W kg<sup>-1</sup>, was achieved using more than 100 g of ECM. Data on the long-term stability of this system were not provided.

A comparison of the long-term stability of different nickel-titanium based ECM-samples is given in Fig. 1<sup>8–11,13,25–33</sup>. For bulk materials, compressive loading shows a significantly better long-term stability than tensile loading<sup>6,9,13,34,35</sup>. The largest values for compressive loading were achieved by Chen et al.<sup>9</sup> and Zhang et al.<sup>13</sup> with more than 10<sup>7</sup> cycles. Porenta et al.<sup>31</sup> used thin-walled tubes, which withstood more than 10<sup>6</sup> cycles under compression, keeping up an adiabatic temperature change of 27 K. The same long-term stability was shown by Hou et al.<sup>11</sup> for additive-manufactured nickel-titanium samples.

Tensile loading on the other hand is more likely to cause premature material failure, since even very small cracks in the ECM lead to local overload and subsequently to crack growth<sup>6,12</sup>.

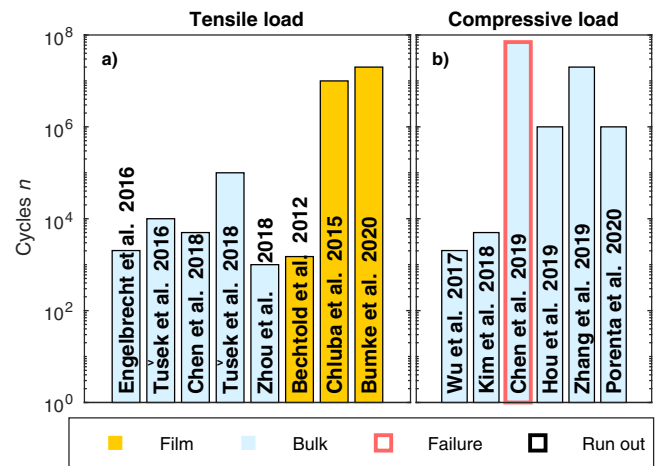


**Fig. 1 Long-term stability of nickel-titanium based alloys quantified in material-test-setups.** Only results of samples that lasted at least 10<sup>3</sup> cycles are shown. The maximum number of cycles measured experimentally are shown for tensile in (a) and compressive loading in (b). Film samples are indicated in yellow. A red frame marks a sample that failed at the end of the test. Bars with a black frame indicate tests that were stopped after a certain number of cycles without detection of material failure (runout). Material composition, sample shape, amount of material, stress, strain, frequency and temperature vary for each sample<sup>8–11,13,25–33</sup>.

However, Chluba et al.<sup>10</sup> achieved 10<sup>7</sup> cycles without material failure in tensile tests with a film of a TiNiCu alloy. Generally, ECS based on films are mainly interesting for miniature scale applications due to the small amount of ECM and the limited cooling power associated with it.

One challenge for compression-based systems with cylindrical or tube-shaped samples is a smaller surface-to-volume ratio compared to tension-based systems, since buckling has to be prevented. Thus, for these systems a large heat transfer coefficient between ECM and heat sink and source is even more important to attain high cooling power densities: The higher the heat transfer coefficient, the smaller the heat transfer surface of the ECM can be.

In this work, we present a system concept, which we call 'active elastocaloric heat pipe' (AEH). The AEH reaches unprecedented long-term stability and cooling power density. The key of this concept is to combine compressive loading of the ECM and latent heat transfer by condensation and evaporation of a fluid (water)<sup>36</sup>.

## Results

**Active elastocaloric heat pipe (AEH).** Passive latent heat transfer is commonly used in heat pipes as well as thermosiphons<sup>37</sup> and was already realized in a magnetocaloric cooling system<sup>38</sup>. Here, a fluid present in both liquid and gaseous state is contained in a hermetically sealed container. All non-condensable gases (nitrogen, oxygen, etc.) have been removed. In such a two-phase system, pressure is a function of temperature, determined by the vapour-pressure curve of the fluid (water)<sup>39</sup>. Thus, if the temperature increases on the container's hot side, water evaporates, leading to an increase in pressure and condensation on the cold side. This way a very fast heat transfer is established. Since water is characterized by very large enthalpy of evaporation, a small amount of water can transfer a great amount of heat, enabling heat transfer coefficients that are orders of magnitude larger than e. g. convective heat transfer.

The AEH consists of several elastocaloric segments, which are thermally connected in series and compressed by a crankshaft

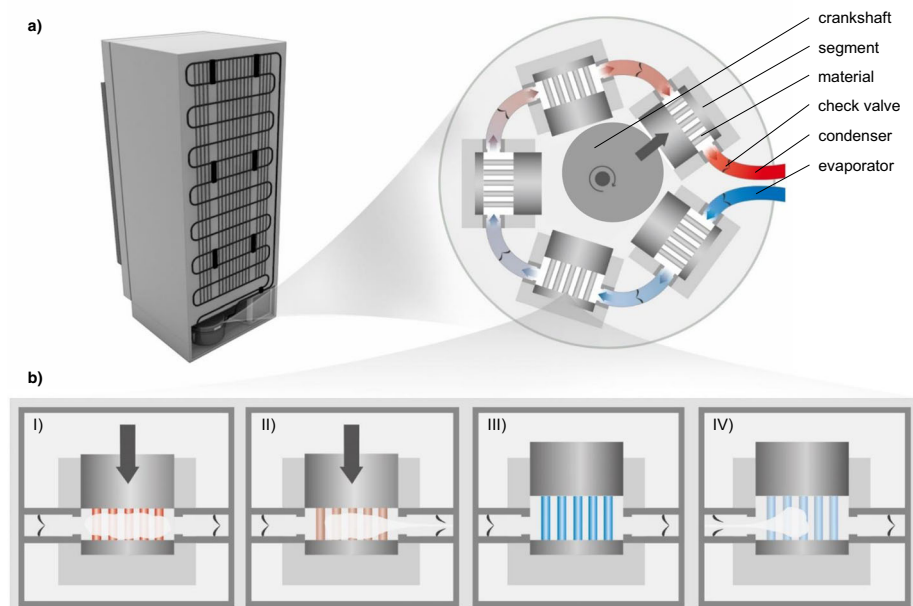


**Fig. 2 Functional schematic of an active elastocaloric heat pipe (AEH).** **a** AEH cooling unit of a refrigerator consisting of five segments connected in series between evaporator and condenser. **b** shows the elastocaloric cycle in only one segment of an AEH: I: The ECM heats up under load. The fluid on the surface of the ECM evaporates, the vapour pressure in this segment increases. II: Caused by the pressure difference between this segment and the next segment, the right check valve opens. Gaseous fluid flows into the next segment. III: By removing the load, the ECM cools down. IV: Fluid from the gaseous phase condenses, the vapour pressure decreases to a level below the pressure in the previous segment. The left check valve opens and gaseous fluid flows into the segment.

(Fig. 2a). Each of these hermetically sealed segments contains the ECM, the heat transfer fluid and passive check valves. By alternately compressing the ECM in each segment, a unidirectional gas flow is established and heat is transferred from the evaporator (heat source) to the condenser (heat sink) (Fig. 2b). The check valves on each side of the segments direct the gaseous fluid and thereby the heat flow. The valves open and close due to the temperature-induced pressure change in each segment. Liquid fluid is accumulated in the condenser and transferred back to the evaporator through a throttle like in a conventional refrigeration system.

A single stage AEH-system was built using six commercially available tubes of  $\text{Ni}_{56,25}\text{Ti}_{43,73}$  showing an adiabatic temperature change of  $17.2 \pm 0.5$  K at a compressive stress of  $1234 \pm 7.3$  MPa (Supplementary Fig. 1). A total mass of 1.26 g of this material was integrated into the segment. Check valves were used to direct the flow of the heat transfer fluid (water)<sup>40</sup>. The condenser was connected to a thermal bath for temperature control at 21 °C, while the evaporator was thermally isolated to the environment. A heating wire was wrapped around the evaporator in order to be able to apply a certain heat load to the cold side. The system was characterized at different frequencies and heat loads by measuring the pressure difference between evaporator and condenser. The ECM is compressed along a sinusoidal stress profile with a maximum stress of  $1226 \pm 70$  MPa. During these characterisations the throttle is closed and therefore does not influence the measurement.

**Characterisation of the AEH.** The AEH was characterized for different frequencies and heat loads. A maximum temperature span of 5.6 K for zero load and a maximum cooling power of 7.9 W for zero temperature span, corresponding to a maximum specific cooling power of  $6,270 \text{ W kg}^{-1}$ , was measured for a system frequency of 1.2 Hz. For intermediate values, a linear relationship between temperature span and cooling power was

found (Fig. 3), which is in accordance with the theoretically expected relationship for such a system<sup>41</sup>. After this initial characterization, the system was operated at 10 Hz to exert several millions of load cycles on the ECM.

For a quick test to validate that the system is working without performance losses, review tests were performed at 0.8 Hz with 0 W as well as with 2 W heat load (Fig. 3a). After  $4.5 \times 10^6$  and  $10^7$  cycles, the system was fully characterized again with the same frequencies and heat loads as at the beginning (Fig. 3b).

The system shows a very stable performance with a decrease in maximum temperature span of <8% after 10 million cycles, and no failure of material could be detected.

## Discussion

The long-term stability shown for this AEH-system exceeds that of all other ECSs reported in the literature by orders of magnitude. Furthermore, due to the improved heat transfer, the specific cooling power is improved by one order of magnitude if compared to the compression-based ECS of Qian et al.<sup>23</sup>.

A comparison of long-term stability and cooling power for tensile loaded ECS with the compression-based AEH-system is shown in Fig. 4<sup>10,15,18,20–22,24,42</sup>. It can be seen that two systems show material failure after several hundred cycles, achieving a cooling power of several tens to hundreds of milliwatts<sup>15,18</sup>. Thin-film samples of the TiNiCu-alloy, that showed a long term stability of  $10^7$  cycles in a material test setup<sup>10</sup>, demonstrated a cooling power of 0.222 W in a tension-based ECS built by Brüderlin et al.<sup>22</sup>. Accordingly, bulk samples of NiTi, which lasted 5200 cycles in a material test setup<sup>20</sup>, showed a cooling power of 4.5 W in an ECS built by Tušek et al.<sup>21</sup>.

Compared to these systems, the AEH shows an improvement in both long-term stability and cooling power by orders of magnitude.

The compression-based ECS presented in this work for the first time achieved more than  $10^7$  cycles with only a slight

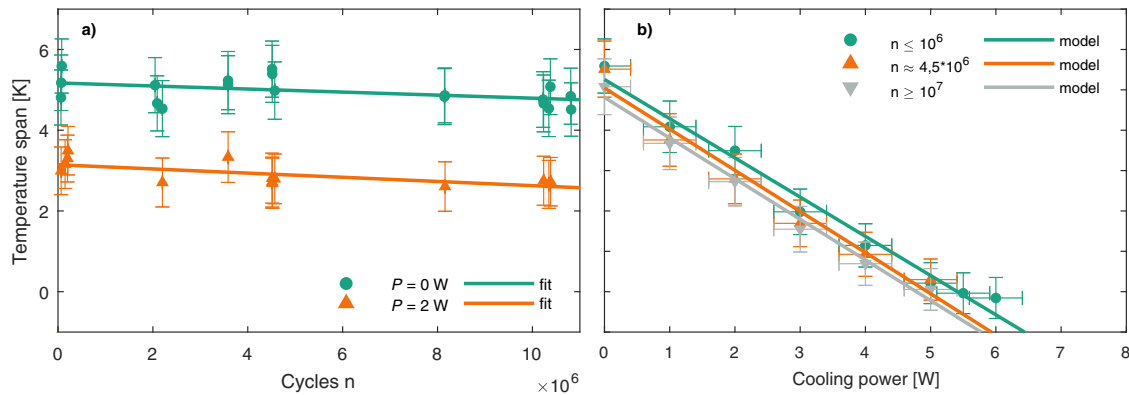


**Fig. 3 Long-term stability of the active elastocaloric heat pipe (AEH).** **a** The temperature span versus the number of cycles  $n$  at a frequency of 0.8 Hz is plotted in green with zero and in orange with 2 W of heating load at the evaporator. The data are in agreement with a linear for the entire measurement series (lines). The linear fit for the maximum temperature span  $\Delta T$  is  $\Delta T = 5.2 \text{ K} - n \cdot 3.8 \cdot 10^{-8} \text{ K}$ , for 2 W it is  $\Delta T = 3.1 \text{ K} - n \cdot 5.2 \cdot 10^{-8} \text{ K}$ . Error bars as calculated as described in the methods. **b** Measurement of the temperature span at different heat loads at a frequency of 0.8 Hz. The data points at the beginning of the long-term measurement are shown in green, after  $4.5 \times 10^6$  cycles in orange and after more than  $10^7$  cycles in grey. The linear fit is expected<sup>41</sup>. The calculation of the errors is given in the methods.

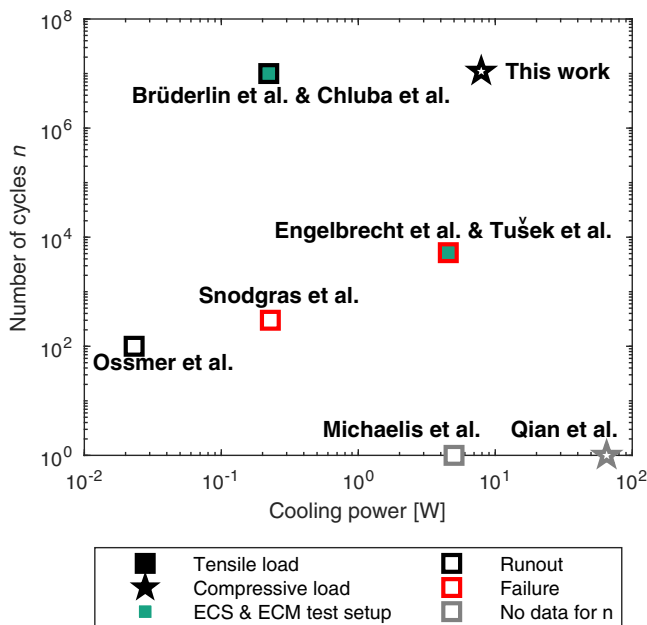


**Fig. 4 Comparison of cooling power and long-term stability of different elastocaloric cooling systems (ECS) or material test setups<sup>10,15,18,20-22,24,42</sup>.** A square indicates tests under tensile load, the star indicates compressive load. A red frame around the data point indicates the value at which the sample in a test failed. A black frame marks tests that were stopped after a certain number of cycles (runout). Data without reported cycle stability are shown in grey. Material composition, sample shape, amount of material, stress, strain, frequency and temperature vary in the results plotted. Both, the work of Brüderlin et al.<sup>22</sup> and Chluba et al.<sup>10</sup> as well as Engelbrecht et al.<sup>20</sup> and Tušek et al.<sup>21</sup> are marked green, since they have demonstrated their long-term stability in a material test setup rather than in an ECS.

performance drop, showing no material failure. This proves that one of the major challenges for elastocaloric cooling on its way to commercialization can be resolved by choosing a compression-based concept for ECSs. At the same time, it was possible to show a cooling power of 7.9 W corresponding to a specific cooling power of  $6,270 \text{ W kg}^{-1}$ , which means nearly one order of magnitude increase compared to the best ECS-systems based on bulk ECMs<sup>21</sup>. This was possible by using latent heat of fluid during

evaporation and condensation for a fast and efficient heat transfer to heat sink and source. By connecting several segments in series, the maximum temperature span of the AEH can be significantly increased in the future. Hereby, the specific cooling capacity approximately scales inversely to the number of cascaded segments<sup>41,43</sup>, while the second law efficiency of the system is independent from the number of stages.

In this work the loading of the elastocaloric material was done by compression. It is also possible to adapt the AEH concept to tensile loading, potentially leading to even larger specific cooling capacities.

Thus, latent heat transfer in elastocaloric cooling systems can pave the way to many applications for an energy-efficient and environmentally friendly alternative to existing cooling technologies.

## Methods

**Material.** The ECM used in the setup are nickel-titanium tubes with 56.25 wt% nickel and 43.73 wt% titanium (alloy contents below 0.03% are not listed) with an austenite finishing temperature of  $A_f = -1.4 \text{ }^\circ\text{C}$  and were purchased from EUROFLEX GmbH. According to manufacturer's specifications, the tubes have an outer diameter of  $2.40 \pm 0.01 \text{ mm}$  and an inner diameter of  $1.45 \pm 0.04 \text{ mm}$ . The tubes were cut and polished to a length of  $11.005 \pm 0.010 \text{ mm}$ . The specific heat capacity of the alloy is  $540 \pm 90 \text{ J kg}^{-1} \text{ K}^{-1}$  and was measured by Ingplus GmbH in a differential scanning calorimeter.

Before measuring the adiabatic temperature change, the ECM was trained over more than 2,000 cycles. The adiabatic temperature span was then measured in a self-made experimental material characterization setup, giving  $17.2 \pm 0.5 \text{ K}$  for loading and  $11.9 \pm 0.5 \text{ K}$  for unloading for a compressive stress of  $1234 \pm 7 \text{ MPa}$  (Supplementary Fig. 1). The uncertainty of the temperature results from the specifications of the thermocouple manufacturer and the uncertainty of the stress results from the manufacturer's specifications of the force sensor from HBM GmbH.

**Setup of single-stage AEH-system.** Supplementary Fig. 2a shows the experimental setup for long-term-stability measurements of the single-stage AEH-system. The system consists of a crankshaft that compresses one elastocaloric segment, which is located between evaporator and condenser. The eccentricity the crankshaft is  $300 \text{ } \mu\text{m}$  with a tolerance of  $\pm 30 \text{ } \mu\text{m}$ . The force is measured with the sensor C10 Force Sensor from Hottinger Baldwin Messtechnik GmbH and determines the maximum stress. The maximum load is  $F_{\text{max}} = 21 \text{ kN}$  with a reading accuracy of 1 kN. This corresponds to a maximum stress  $\sigma_{\text{max}}$  of  $1226 \pm 70 \text{ MPa}$ .

Supplementary Fig. 2b shows the elastocaloric segment consisting of two connectors holding the check valves (Supplementary Fig. 2d) and a bellow, where the compressive force can be applied to. Six tubes of  $\text{Ni}_{56,25}\text{Ti}_{43,73}$  were fixed by sample holders to prevent them from slipping (Supplementary Fig. 2c) and are integrated into the segment.

The check valves (Supplementary Fig. 2d) separate the evaporator and condenser from the segment. With water as heat transfer fluid, a temperature difference of 1 K across the check valve results in a heat flow of 166 W in forward



direction. For AEH-systems aiming for larger cooling power, these check valves can become a limiting factor. In that case, check valves with a larger cross-section need to be implemented. In the backward direction, the heat flow for a temperature difference of  $-1$  K is  $0.01$  W<sup>40</sup>.

**Preparation of heat transfer fluid.** In order to have fast heat transfer by evaporation and condensation of the water, all non-condensable gases have to be removed from the system. For this purpose, the water is frozen and the gas phase is removed using a vacuum pump from Gardner Denver Thomas GmbH. After melting and refreezing the water, this procedure is repeated five times in order to remove non-condensable gases that were dissolved in the solid phase.

**Temperature measurement in two-phase region.** In the two-phase region, direct temperature measurements using e.g., thermocouples are inaccurate due to poor heat conduction of the thin gas atmosphere. Therefore, pressure sensors (CMR 371, 1,000 hPa F.S.) from Pfeiffer Vacuum GmbH are used for pressure measurement. These pressure data  $p$  in bar can be converted into temperatures  $T$  in K using the Antoine equation<sup>39</sup>:

$$T = \frac{1838.675 \text{ K}}{5.40221 - \log_{10}\left(\frac{p}{\text{bar}}\right)} + 31.737 \text{ K.} \quad (1)$$

Although sensor specified for measurement in the two-phase region of water were used, an offset between the pressure sensors was observed, apparently due to some condensation of the liquid on the sensors membranes. To quantify this offset and account for the subsequent measurement uncertainties, measurements were made with the two pressure sensors in a contiguous volume. The results of these measurements are listed in (Supplementary Table 1). The mean value of these differences is  $p_d = -0.72$  mbar, its standard deviation to  $S_p = -0.17$  mbar.

In the experiments of the elastocaloric system, the pressure values were shifted by half of this mean pressure difference, and the measurement uncertainty was quantified using its standard deviation. The measurement uncertainties of the temperatures were then determined using Gaussian error propagation.

**Uncertainty of thermal load.** The thermal load on the cold side is applied by an electrical wire, which is heating the evaporator. Since the electrical resistance of the wire and the applied current and voltage can be quantified by large accuracy, the main source of uncertainty of the thermal load on the cold side is based on an insufficient isolation of the evaporator. Hereby, the maximum heat loss through this isolation occurs, when the temperature difference between evaporator and environment is maximal, i.e. for  $\Delta T_{\text{max}} = 5.6$  K. With an estimate of the thermal resistance of the isolation  $R_{\text{th}}^{\text{iso}}$ , this maximum heat loss is given by  $Q_{\text{max}}^{\text{iso}} = \frac{\Delta T_{\text{max}}}{R_{\text{th}}^{\text{iso}}}$ . For the isolation, polyethylene foam with a thermal conductivity  $\lambda = 0.04$  W m<sup>-1</sup> K<sup>-1</sup> is used, in which the evaporator is embedded. A cross-sectional view of the evaporator with insulation is shown in Supplementary Figure 3. The evaporator has the shape of a tube with a radius  $r_i = 8$  mm and length  $L = 0.3$  m. The evaporator is wrapped into the polyethylene insulation with a thickness of 15 mm. Thus, the outer radius of the insulation is  $r_a = 23$  mm, the inner radius  $r_i = 8$  mm. The thermal resistance of this concentric, tube-shaped isolation is then given by:

$$R_{\text{th}}^{\text{iso}} = \frac{\ln\left(\frac{r_a}{r_i}\right) - \ln\left(\frac{r_i}{\text{mm}}\right)}{2\pi\lambda L} = 14 \frac{\text{K}}{\text{W}}. \quad (2)$$

This results in a maximum heat loss through the isolation of  $Q_{\text{max}}^{\text{iso}} = 0.4$  W, giving an upper estimate of the uncertainty of the thermal load.

**Surface to volume ratio determined by critical stress under compressive load of ECM.** When the ECM is loaded under compression, one has to make sure that no buckling of the ECM occurs. According to Euler's buckling modes, the critical load  $F_{\text{crit}}$  for a cylinder is given by  $F_{\text{crit}} = \frac{4\pi^2 EI}{l^2}$ .  $E$  is the Young's modulus,  $I = \pi r^4/4$  the area moment of inertia,  $r$  the radius and  $l$  the length of the ECM. With the mass of the cylinder  $m = \rho \pi r^2 l$  and the density  $\rho$ , the radius can be expressed as  $r = \frac{2m}{\rho A}$  and the length as  $l = \frac{\rho A^2}{4\pi m^2}$ , where  $A = 2\pi r l$  denotes the surface area of the ECM-cylinder used for heat transfer.

Now, the critical stress  $\sigma_{\text{crit}} = \frac{F_{\text{crit}}}{\pi r^2}$  can be expressed as follows:

$$\sigma_{\text{crit}} = \frac{4\pi^2 EI}{l^2 \pi r^2} = \frac{64E\pi^4 m^4}{\rho^4 A^6} \sim \frac{m^4}{\rho^4 A^6}. \quad (3)$$

The critical stress is inversely proportional to the surface area of the cylindrical sample  $A$  to the power of six.

**Additional measurement results.** As an example for the transient pull-down when the system is started, temperature data of evaporator and condenser are shown in Supplementary Figure 4 for a system frequency of 0.8 Hz.

Supplementary Fig. 5 shows the measured steady state temperature span for different applied heat loads of the AEH at the beginning of the long-term measurement at 0.4 Hz, 0.8 Hz, 1.2 Hz and 1.5 Hz. The experimental data are in line with the theoretical model by Hess et al.<sup>41</sup>, which was fitted to the data. There

it is shown that the heat flux is linear for frequencies smaller than the cut-off frequency. For higher frequencies the heat flow goes into saturation. The heat flux can be expressed as a function of the frequency, the cut-off frequency and the maximum heat flux. A maximum cooling power of 7.9 W at a temperature span of 0 K for a frequency of 1.2 Hz was measured. This corresponds to a maximum specific cooling power of 6270 W kg<sup>-1</sup>.

## Data availability

The data that support the findings of this study are available from the corresponding author upon reasonable request.

Received: 15 March 2021; Accepted: 27 July 2021;

Published online: 24 August 2021

## References

1. The Future of Cooling – Analysis - IEA. Available at <https://www.iea.org/reports/the-future-of-cooling> (2018).
2. Umweltbundesamt. EU Regulation concerning fluorinated greenhouse gases. Available at <https://www.umweltbundesamt.de/en/topics/climate-energy/fluorinated-greenhouse-gases-fully-halogenated-cfcs/statutes-regulations/eu-regulation-concerning-fluorinated-greenhouse> (2020.000Z).
3. Comm/dg/unit. Paris Agreement - Climate Action - European Commission. Available at [https://ec.europa.eu/clima/policies/international/negotiations/paris\\_en](https://ec.europa.eu/clima/policies/international/negotiations/paris_en) (2020).
4. Kitanovski, A. et al. Magnetocaloric Energy Conversion. From Theory to Applications (Springer International Publishing, Cham, s.l., 2015).
5. Goetzler, W., Zogg, R., Young, J. & Johnson, C. Energy savings potential and RD&D opportunities for non-vapor-compression HVAC technologies. Navigant Consulting Inc., prepared for US Department of Energy (2014).
6. Kabirifar, P. et al. Elastocaloric cooling: state-of-the-art and future challenges in designing regenerative elastocaloric devices. *SV-JME* **65**, 615–630 (2019).
7. Wang, R. et al. Torsional refrigeration by twisted, coiled, and supercoiled fibers. *Science* **366**, 216–221 (2019).
8. Bumke, L. et al. Cobalt gradient evolution in sputtered TiNiCuCo films for elastocaloric cooling. *Phys. Status Solidi B* **255**, 1700299 (2018).
9. Chen, J., Zhang, K., Kan, Q., Yin, H. & Sun, Q. Ultra-high fatigue life of NiTi cylinders for compression-based elastocaloric cooling. *Appl. Phys. Lett.* **115**, 93902 (2019).
10. Chluba, C. et al. Ultralow-fatigue shape memory alloy films. *Science* **348**, 1004–1007 (2015).
11. Hou, H. et al. Fatigue-resistant high-performance elastocaloric materials made by additive manufacturing. *Science* **366**, 1116–1121 (2019).
12. Hou, H. et al. Overcoming fatigue through compression for advanced elastocaloric cooling. *MRS Bull.* **43**, 285–290 (2018).
13. Zhang, K., Kang, G. & Sun, Q. High fatigue life and cooling efficiency of NiTi shape memory alloy under cyclic compression. *Scr. Mater.* **159**, 62–67 (2019).
14. Bruederlin, F., Ossmer, H., Wendler, F., Miyazaki, S. & Kohl, M. SMA foil-based elastocaloric cooling: from material behavior to device engineering. *J. Phys. D: Appl. Phys.* **50**, 424003 (2017).
15. Ossmer, H., Chluba, C., Kauffmann-Weiss, S., Quandt, E. & Kohl, M. TiNi-based films for elastocaloric microcooling— Fatigue life and device performance. *APL Mater.* **4**, 64102 (2016).
16. Schmidt, M., Schuetze, A. & Seelecke, S. Scientific test setup for investigation of shape memory alloy based elastocaloric cooling processes. *Int. J. Refrig.* **54**, 88–97 (2015).
17. Ulpiani, G. et al. Upscaling of SMA film-based elastocaloric cooling. *Appl. Therm. Eng.* **180**, 115867 (2020).
18. Snodgrass, R. & Erickson, D. A multistage elastocaloric refrigerator and heat pump with 28 K temperature span. *Sci. Rep.* **9**, 18532 (2019).
19. Kirsch, S.-M. et al. NiTi-based elastocaloric cooling on the macroscale: from basic concepts to realization. *Energy Technol.* **6**, 1567–1587 (2018).
20. Engelbrecht, K. et al. A regenerative elastocaloric device: experimental results. *J. Phys. D: Appl. Phys.* **50**, 424006 (2017).
21. Tušek, J. et al. A regenerative elastocaloric heat pump. *Nat. Energy* **1**, 10 (2016).
22. Bruederlin, F. et al. Elastocaloric cooling on the miniature scale: a review on materials and device engineering. *Energy Technol.* **6**, 1588–1604 (2018).
23. Qian, S. et al. A review of elastocaloric cooling. Materials, cycles and system integrations. *Int. J. Refrig.* **64**, 1–19 (2016).
24. Qian, S. et al. Design of a hydraulically driven compressive elastocaloric cooling system. *Sci. Technol. Built Environ.* **22**, 500–506 (2016).
25. Bechtold, C., Chluba, C., Lima de Miranda, R. & Quandt, E. High cyclic stability of the elastocaloric effect in sputtered TiNiCu shape memory films. *Appl. Phys. Lett.* **101**, 91903 (2012).

26. Tušek, J. et al. Elastocaloric effect vs fatigue life: exploring the durability limits of Ni-Ti plates under pre-strain conditions for elastocaloric cooling. *Acta Materialia* **150**, 295–307 (2018).
27. Tušek, J., Engelbrecht, K. & Pryds, N. Elastocaloric effect of a Ni-Ti plate to be applied in a regenerator-based cooling device. *Sci. Technol. Built Environ.* **22**, 489–499 (2016).
28. Chen, H. et al. Stable and large superelasticity and elastocaloric effect in nanocrystalline Ti-44Ni-5Cu-1Al (at%) alloy. *Acta Materialia* **158**, 330–339 (2018).
29. Zhou, M., Li, Y.-S., Zhang, C. & Li, L.-F. Elastocaloric effect and mechanical behavior for NiTi shape memory alloys. *Chin. Phys. B* **27**, 106501 (2018).
30. Kim, Y., Jo, M.-G., Park, J.-W., Park, H.-K. & Han, H. N. Elastocaloric effect in polycrystalline Ni 50 Ti 45.3 V 4.7 shape memory alloy. *Scr. Materialia* **144**, 48–51 (2018).
31. Porenta, L. et al. Thin-walled Ni-Ti tubes under compression: ideal candidates for efficient and fatigue-resistant elastocaloric cooling. *Appl. Mater. Today* **20**, 100712 (2020).
32. Engelbrecht, K. et al. Effects of surface finish and mechanical training on Ni-Ti sheets for elastocaloric cooling. *APL Mater.* **4**, 64110 (2016).
33. Wu, Y., Ertekin, E. & Sehitoglu, H. Elastocaloric cooling capacity of shape memory alloys - Role of deformation temperatures, mechanical cycling, stress hysteresis and inhomogeneity of transformation. *Acta Mater.* **135**, 158–176 (2017).
34. Sehitoglu, H., Wu, Y. & Ertekin, E. Elastocaloric effects in the extreme. *Scr. Mater.* <https://doi.org/10.1016/j.scriptamat.2017.05.017> (2017).
35. Imran, M. & Zhang, X. Recent developments on the cyclic stability in elastocaloric materials. *Mater. Des.* **195**, 109030 (2020).
36. Bartholome, K., Horzella, J., Mahlke, A., Konig, J. & Vergez, M. Method and apparatus for operating cyclic process-based system. DE201510121657;DE2016 10100596;WO2016EP80461, F25B23/00 (2016).
37. Reay, D. A., Kew, P. A. & McGlen, R. J. Heat Pipes: Theory, Design and Applications. 6th ed. (Butterworth-Heinemann, 2013).
38. Maier, L. M. et al. Active magnetocaloric heat pipes provide enhanced specific power of caloric refrigeration. *Commun. Phys.* **3**, 1–6 (2020).
39. National Institute of Standards and Technology. Water. Available at <https://webbook.nist.gov/cgi/cbook.cgi?ID=C7732185&Mask=4&Type=ANTOINE&Plot=on> (2020).
40. Maier, L. M. et al. Method to characterize a thermal diode in saturated steam atmosphere. *Rev. Sci. Instrum.* **91**, 65104 (2020).
41. Hess, T. et al. Modelling cascaded caloric refrigeration systems that are based on thermal diodes or switches. *Int. J. Refrig.* **103**, 215–222 (2019).
42. Michaelis, N. et al. Investigation of Elastocaloric Air Cooling Potential Based on Superelastic SMA Wire Bundles. Available at [https://www.researchgate.net/publication/344198524\\_INVESTIGATION\\_OF\\_ELASTOCALORIC\\_AIR\\_COOLING\\_POTENTIAL\\_BASED\\_ON\\_SUPERELASTIC\\_SMA\\_WIRE\\_BUNDLES](https://www.researchgate.net/publication/344198524_INVESTIGATION_OF_ELASTOCALORIC_AIR_COOLING_POTENTIAL_BASED_ON_SUPERELASTIC_SMA_WIRE_BUNDLES) (2020).
43. Bruederlin, F., Bumke, L., Quandt, E. & Kohl, M. Cascaded SMA-Film Based Elastocaloric Cooling. 20th International Conference on Solid-State Sensors, Actuators and Microsystems & Eurosensors XXXIII, 1467–1470 (2019).

## Acknowledgements

This work was funded by the Federal Ministry of Education and Research (BMBF) of Germany as part of the ElastoCool project (Grant No. 03VP04670).

## Author contributions

N.B. and A.M. performed the experiments; N.B., A.F. and K.B. analysed the data; N.B., A.F. and L.M.M., interpreted the data; K.B., O.S.W. and T.K. supervised the work; K.B. and O.S.W. acquired funding; and N.B., K.B. and O.S.W. wrote the manuscript. All authors contributed to the interpretation of the data and commented on the manuscript.

## Funding

Open access funding enabled and organized by Projekt DEAL.

## Competing interests

The authors declare no competing interests.

## Additional information

**Supplementary information** The online version contains supplementary material available at <https://doi.org/10.1038/s42005-021-00697-y>.

**Correspondence** and requests for materials should be addressed to N.B. or K.Bé.

**Peer review information** *Communications Physics* thanks Suxin Qian, Neil Mathur and the other, anonymous, reviewer(s) for their contribution to the peer review of this work. Peer reviewer reports are available.

**Reprints and permission information** is available at <http://www.nature.com/reprints>

**Publisher's note** Springer Nature remains neutral with regard to jurisdictional claims in published maps and institutional affiliations.



**Open Access** This article is licensed under a Creative Commons Attribution 4.0 International License, which permits use, sharing, adaptation, distribution and reproduction in any medium or format, as long as you give appropriate credit to the original author(s) and the source, provide a link to the Creative Commons license, and indicate if changes were made. The images or other third party material in this article are included in the article's Creative Commons license, unless indicated otherwise in a credit line to the material. If material is not included in the article's Creative Commons license and your intended use is not permitted by statutory regulation or exceeds the permitted use, you will need to obtain permission directly from the copyright holder. To view a copy of this license, visit <http://creativecommons.org/licenses/by/4.0/>.

© The Author(s) 2021